International Journal of Nanomedicine

Dovepress
open access to scientific and medical research

Open Access Full Text Article

ORIGINAL RESEARCH

A SERS Biosensor Based on Functionalized Au-SiNCA Integrated with a Dual Signal Amplification Strategy for Sensitive Detection of Telomerase Activity During EMT in Laryngeal Carcinoma

Yuexing Gu[1,2,*], Yan Li[3,*], Shengjie Ge[1,2], Wenbo Lu[4], Yu Mao[1,2], Miao Chen[1,2], Yayun Qian[1,2]

[1]Institute of Translational Medicine, Medical College, Yangzhou University, Yangzhou, People's Republic of China; [2]Jiangsu Key Laboratory of Integrated Traditional Chinese and Western Medicine for Prevention and Treatment of Senile Diseases, Yangzhou University, Yangzhou, People's Republic of China; [3]Department of Obstetrics and Gynecology, The Second People's Hospital of Taizhou City, Taizhou, People's Republic of China; [4]Shanxi Normal University, College of Chemistry and Material Science, Linfen, People's Republic of China

*These authors contributed equally to this work

Correspondence: Yayun Qian, Email yyqian@yzu.edu.cn

Purpose: This paper aims to construct a surface-enhanced Raman spectroscopy (SERS) biosensor based on functionalized Au-Si nanocone arrays (Au-SiNCA) using a dual signal amplification strategy (SDA-CHA) to evaluate telomerase activity during epithelial-mesenchymal transition (EMT) in laryngeal carcinoma (LC).

Methods: A SERS biosensor based on functionalized Au-SiNCA was designed with an integrated dual-signal amplification strategy to achieve ultrasensitive detection of telomerase activity during EMT in LC patients.

Results: Labeled probes (Au-AgNRs@4-MBA@H_1) and capture substrates (Au-SiNCA@H_2) were prepared by modifying hairpin DNA and Raman signal molecules. Using this scheme, telomerase activity in peripheral mononuclear cells (PMNC) could be successfully detected with a limit of detection (LOD) as low as 10^{-6} IU/mL. In addition, biological experiments using BLM treatment of TU686 effectively mimicked the EMT process. The results of this scheme were highly consistent with the ELISA scheme, confirming its accuracy.

Conclusion: This scheme provides a reproducible, selective, and ultrasensitive assay for telomerase activity, which is expected to be a potential tool for the early screening of LC in future clinical applications.

Keywords: surface-enhanced Raman scattering, telomerase, laryngeal carcinoma, epithelial-mesenchymal transition, Au-SiNCA

Introduction

Laryngeal carcinoma (LC), the second most common head and neck malignancy worldwide, has a high incidence, significant malignancy, and poor prognosis, with a 5-year survival rate of 40%.[1,2] Surgical resection is the only possible radical treatment for LC, and patients with LC are often diagnosed with advanced stages with the development of lymph node metastases due to the lack of major-specific early clinical manifestations.[3,4] Epithelial-mesenchymal transition (EMT) is the process through which cancer cells acquire invasive mesenchymal cell-like properties, resulting in metastasis from the primary tumor site to adjacent tissues or even distal sites and ultimately leading to resistance to therapeutic intervention; thus, a systematic exploration of EMT could deepen our understanding of LC tumorigenesis and progression, which may assist in early diagnosis and effective treatment.[5,6] Telomerase is a reverse transcriptase that carries its templates and maintains telomere length by synthesizing telomeric DNA repeats, enabling the cells' unlimited

Received: 8 March 2023
Accepted: 9 May 2023
Published: 15 May 2023

proliferation. While the content of telomerase in normal cells is low due to transcriptional inhibition, researchers have proved that the mechanism of telomerase overexpression and reactivation becomes an essential factor leading to unlimited cell proliferation and malignant transformation during the EMT process of LC.[7,8] Thus, telomerase is considered an important diagnostic and prognostic cancer biomarker, and efficient determination of telomerase activity is significant.

Polymerase chain reaction (PCR)-based telomere repeats amplification protocol (TRAP) is the widespread conventional method for telomerase activity detection; however, its disadvantages are also protruding, such as long detection time and false-positive results.[9–11] Although various methods, including electrochemistry, fluorescence, and colorimetric, have achieved satisfactory sensitivity and specificity, the requirement of complicated manipulation and elaborate instruments significantly limits their application in clinical research.[12,13] Benefitting from the characteristics of high-resolution, fingerprint identification, rapid analysis process, and non-destruction, surface-enhanced Raman scattering (SERS), a spectrum analysis technology bridged between Raman spectroscopy and nanotechnology, has attracted increased interest in bioanalytical applications.[14,15] In principle, the main contributor of SERS is thought to be the electromagnetic enhancement of adjacent noble metal nanostructure surfaces (also called "hot spots") induced by localized surface plasmon resonance (LSPR) which is generated when the frequency of the incident photon matches the overall vibration frequency of the electrons conducted by the precious metal nanoparticles or metal island.[16,17] Therefore, a wide range of nanostructure-based SERS-active substrates and probes have been developed to achieve strong Raman signals.[18–20] Attributed to the lattice-matching characteristics of Au and Ag, researchers have proved that Au-Ag core-shell nanostructures have outstanding optical performance.[21–23] Among these, Au-Ag core-shell nanorods (Au-AgNRs), as an anisotropic nanostructure, have gained widespread attention due to their sharper plasma peaks and stronger interparticle near-field coupling effect.[24,25] In particular, Au-AgNRs with absorption in the near-infrared region has a higher penetration depth, providing deep tissue penetration that can be widely used for photothermal therapy or bioimaging. In addition, the ordered Au-Si nanocone arrays (Au-SiNCA) prepared by colloidal sphere template-assisted etching can ensure a uniform distribution of hot spots and adsorbed target molecules (or analytes) on the chip when used as SERS substrates, achieving excellent signal reproducibility and accurate quantitative SERS detection, which has a wide range of prospects in the field of molecular detection.[26]

Due to the low expression level of telomerase during EMT in early LC patients, traditional detection methods cannot accurately identify it. To this end, in recent years, a series of DNA signal amplification strategies such as polymerase chain reaction (PCR), loop-mediated isothermal amplification (LAMP), and rolling circle amplification (RCA) have been introduced in SERS detection to improve the analytical sensitivity further.[27–29] Among them, strand displacement amplification (SDA) uses the principle of entropy-driven by conformational change, in which the weakly bound single-stranded DNA is replaced by the strongly bound single-stranded DNA, and the target is amplified exponentially in this cycle to achieve the amplification effect.[30,31] Catalyzed hairpin self-assembly (CHA) can amplify nucleic acid sequences to achieve signal amplification without the help of enzymes at room temperature, showing excellent sensitivity and specificity.[32,33] Currently, most people use a single signal amplification strategy, but the method still meets the detection criteria in the face of low-abundance substances.[34–36] Therefore, a dual signal amplification strategy integrating SDA and CHA (SDA-CHA) is expected to be an effective method to improve the performance of telomerase activity analysis during EMT in LC patients.

Herein, a novel biosensing platform for telomerase detection based on SDA-CHA dual-signal amplification strategy and functionalized Au-SiNCA capture SERS probes (Au-AgNRs) to generate signal enhancement was constructed (Scheme 1). First, the PS microsphere templates were prepared into highly ordered Au-SiNCA by reactive ion etching (RIE) and magnetron sputtering deposition techniques. Hairpin $DNA_2(H_2)$ was used to modify Au-SiNCA to obtain functionalized capture substrates. Subsequently, Au-AgNRs were modified with 4-MBA and hairpin DNA_1 (H_1) as SERS nanoprobes. During detection, telomerase precursors can generate repeating sequences (TTAGGG) at the ends in the presence of telomerase and dNTP and trigger the SDA reaction in the presence of combined strand (DS_1) and single strand (S_4), cyclically generating a large number of single strands (S_2), causing the first signal amplification. Next, the released single-chain S_2 hybridizes with H_1 modified on Au-AgNRs and is captured by hybridization with H_2 on functionalized Au-SiNCA, allowing the signal to be amplified again (CHA reaction). Based on this principle, the activity of telomerase during EMT was

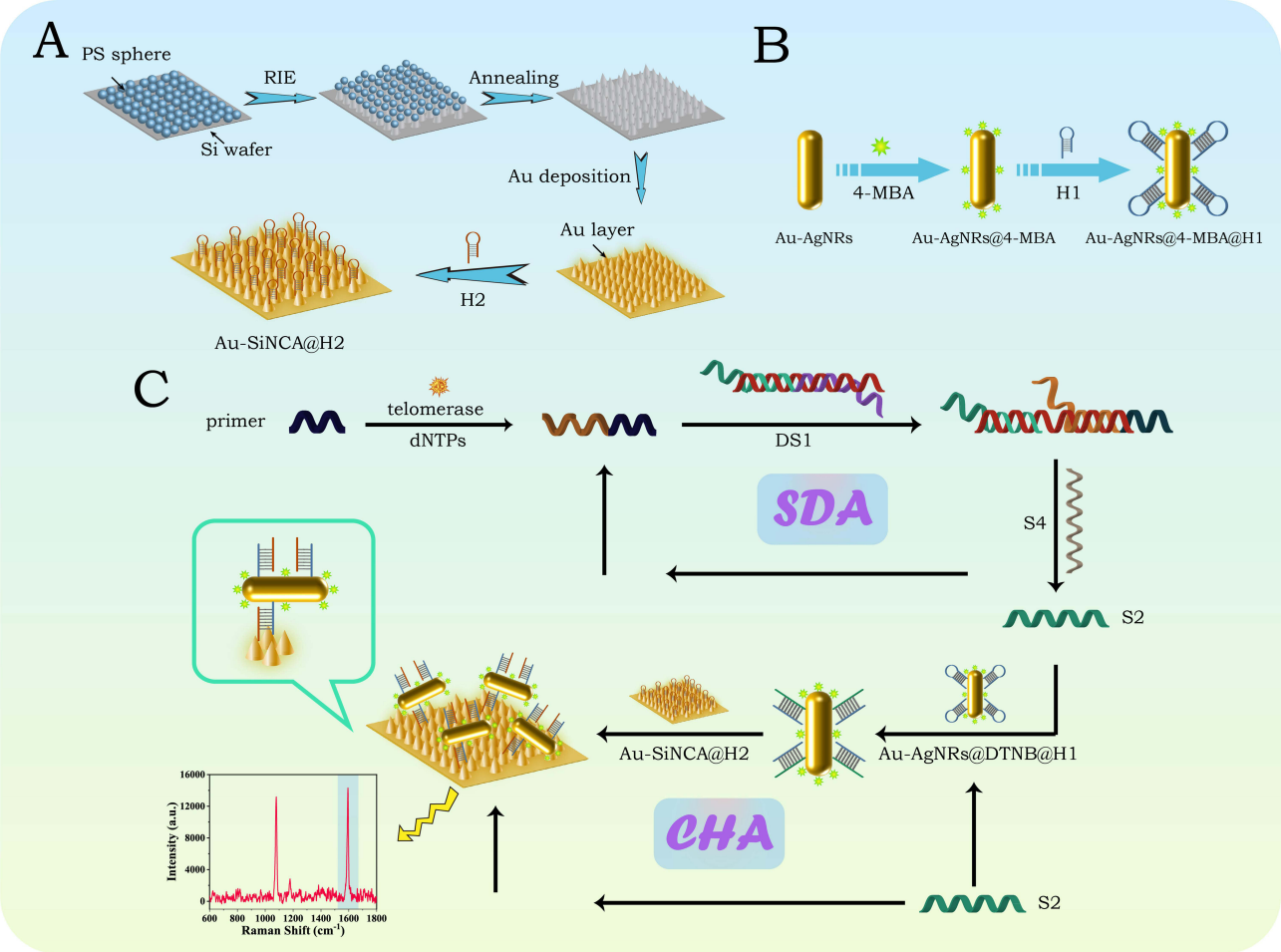

Scheme 1 (**A**) Preparation of the SERS capture substrate; (**B**) Synthesis of the SERS nanoprobes; (**C**) Design principles of telomerase biosensors.

analyzed, and ELISA verified the feasibility. The biosensor provides high specificity and sensitivity for telomerase detection by combining functionalized Au-SiNCA capture Au-AgNRs with a dual signal amplification strategy.

Materials and Methods

Materials

Hexadecyl trimethyl ammonium chloride (CTAC), hexadecyl trimethyl ammonium bromide (CTAB), citric acid, chloroauric acid tetrahydrate ($HAuCl_4$), sodium borohydride ($NaBH_4$), silver nitrate ($AgNO_3$), hydrochloric acid (HCl), ascorbic acid (AA), 4-Mercaptobenzoic acid (4-MBA), triphenylphosphine (TPP), 1-ethyl-3-(3-dimethylaminopropyl) carbodiimide (EDC), N-hydroxysuccinimide (NHS), bleomycin (BLM), and polystyrene sphere (PS) suspension (5 wt%) (120 nm) were all purchased from Sinopharm Chemical Reagent Suzhou Co. Sulfur hexafluoride (SF_6) etching gas was purchased from Nanjing Special Gas Factory Co. The nucleotide sequences used in the experiments were synthesized by Sangon Biotech (Table S1). The resistivity of the deionized water used in the experiments was 18.2 MΩ cm^{-1} at 25 °C. Human peripheral blood specimens and TU686 cells were obtained from the School of Clinical Medicine of Yangzhou University and approved by the Ethics Committee of the School of Clinical Medicine of Yangzhou University (YXYLL-2022-01).

Sample Collection and Processing

Peripheral mononuclear cells (PMNC) were isolated from human peripheral blood samples (LC patients) using Ficoll density gradient centrifugation (720 g, 20 min), then washed 3 times with phosphate buffer and precipitated by low-speed

centrifugation. Then, centrifugation was continued (16,000 g, 20 min) to lyse PMNC, and the supernatant was extracted and frozen in liquid nitrogen and stored at −70 °C. The use of peripheral blood samples was approved by the Ethics Committee of the Medical College of Yangzhou University (YXYLL-2022-01), and all subjects signed an informed consent form.

Fabrication of Functionalized Au-SiNCA

Au-SiNCA was prepared by a PS colloidal sphere template-assisted reactive ion etching (RIE) process combined with a magnetron sputtering deposition technique. First, a uniform PS colloidal sphere monolayer template was prepared on the silicon wafer by the air–water interface self-assembly method. Then, the PS colloidal sphere monolayer templates were heated at 70 °C for 20 min, and the PS colloidal sphere template-covered silicon wafers were etched with SF_6 plasma in the RIE machine for 150 s (power 200 W, gas flow rate 60 sccm). Then, highly ordered silicon nanocone arrays were obtained by rinsing with ethanol and annealing at 600 °C for 2 h to remove the residual PS colloidal spheres. Finally, a thin Au film was sputter-deposited on the Si nanocone arrays using a VTC-16-SM magnetron sputterer at a deposition rate of 0.5 nm/s to obtain the prepared Au-SiNCA. Next, to prepare functionalized Au-SiNCA, hairpin DNA_2 (H_2) was first activated using the newly prepared TECP buffer (100 mL, 1 mM). Then, the synthesized Au-SiNCA was immersed in the solution containing activated H_2 and dried after 12 h of reaction to obtain the functionalized Au-SiNCA.

Synthesis of Au–AgNRs

Au-AgNRs were prepared using the seed-mediated growth method. First, 5.2 mL of CTAC (100 mM), 3.5 mL of citric acid (20 mM), 0.25 mL of $HAuCl_4$ (10 mM), and 3 mL deionized water were mixed and stirred (700 r/min), followed by 0.25 mL of $NaBH_4$ (25 mM) in ice water and heated at 80 °C for 4 h to obtain the Au seed solution. Next, 10 mL of CTAB (100 mM), 0.1 mL of $AgNO_3$ (10 mM), 0.2 mL of HCl (1 M), and 0.1 mL of AA (100 mM) were mixed well, and 450 μL of the above Au seed solution was added while stirring, and the reaction was carried out at room temperature for 2 h. After centrifugation (9000 r/min, 10 min), Au-AgNRs seed solution was obtained. Finally, the above Au-AgNRs seed solution was dispersed into 30 mL of CTAC (80 mM) solution, and 500 μL of $AgNO_3$ (10 mM) and 250 μL of AA (100 mM) were added sequentially, heated at 70 °C for 3 h, centrifuged at 9000 r/min for 10 min. Deionized water was re-dissolved to obtain Au-AgNRs.

Preparation of SERS Nanoprobes

4-MBA was used as a signal marker molecule. Briefly, 200 μL of 4-MBA (2 mM) was added to 4 mL of Au-AgNRs and stirred for 60 min at 25 °C and 700 r/min to obtain Au-AgNRs@4-MBA. Next, newly prepared TECP buffer (100 mL, 1 mM) was used to activate hairpin DNA_1 (H_1), and the activated H_1 was added to Au-AgNRs@4-MBA solution, mixed for 10 h, and then dispersed into 100 μL of BSA solution (1 wt%) and incubated for 1 h. Purification treatment (8000 r/min, 10 min) was performed to obtain Au-AgNRs@4-MBA@H_1.

Telomere Extension Cycle Amplification Reaction

1.0×10^{-6} IU/mL of telomerase extract was added to 200 μL of an extension solution containing 0.5 mM dNTPs and 1 nM extension solution (20 mM Tris-HCl, 4 mM $MgCl_2$, 1 mM EGTA, 60 mM KCl, 0.05% Tween 20) and then incubated in a shaker at 37 °C for 90 min, and the reaction was stopped by reacting at 90 °C for 10 min. Next, 50 μL, 5.0×10^{-7} M single-stranded DNA (S_1, S_2, and S_3) was mixed well and incubated at 37 °C for 2 h to form complementary double-stranded DNA (DS_1). The above telomerase extension product was then added to the DS_1-containing solution with 5.0×10^{-7} M single-stranded DNA (S_4) and incubated for 85 min to allow the strand replacement reaction to proceed sufficiently to displace a large amount of S_2. To allow the CHA reaction, Au-AgNRs@4-MBA@H_1 was added to the above-generated S_2-containing solution, mixed homogeneously, and dropwise to the functionalized Au-SiNCA to cause the CHA reaction to occur, generating a large amount of H_1-H_2.

Measurements and Characterization Techniques

A Renishaw inVia Raman spectrometer measured Raman spectra under a 785 nm excitation laser (laser power of 5 mW, spot of 2 mm, and acquisition time of 10s for each spectrum). Three replicate experiments were performed to obtain spectra from three different sites for each sample and were calibrated using WiRE Raman software version 3.3. SEM imaging of Au-SiNCA was performed using an S-4800II field emission scanning electron microscope (SEM). Tecnai 12 transmission electron microscope (TEM) was used to perform TEM imaging of Au-AgNRs. High-resolution transmission electron microscopy (HRTEM) images and selected area electron diffraction (SAED) images were obtained by a Tecnai G2F30 S-TWIN field emission transmission electron microscope (USA). Ultraviolet-visible-near infrared (UV-Vis-NIR) absorption spectra were obtained by a UV absorption spectrometer (USA).

Results and Discussions

Characterization of Au-SiNCA

From the SEM images of Au-SiNCA (Figure 1A and B), it can be seen that Au-SiNCA was composed of pyramidal structural units with a period of 200 nm and was uniformly ordered in an ordered hexagonal pattern. In order to prove the uniformity of the Raman signal based on Au-SiNCA, it was soaked in 10^{-8} M TPP solution. After drying, the SERS mapping (Figure 1C) was obtained after being excited by a laser with a wavelength of 785 nm. The Raman spectra of 10 points were randomly selected to obtain the average spectrum (Figure 1E and F) the characteristic peak intensity at 998 cm^{-1} (phenyl n1 mode),[37] the obtained Raman spectra have similar spectral shapes, but there are slight differences in peak intensities. The RSD value of the intensity was only 7.36%. Therefore, the structures and hotspots on this chip are uniformly distributed at the scale of the incident laser spot. The enhancement factor (EF) of Au-SiNCA was calculated according to the following expression: $EF = (I_S/C_S) / (I_R/C_R)$, where I_S and I_R refer to the peak intensities of TPP molecules on the Au-SiNCA and Si wafer, respectively, C_S and C_R refer to the concentration of TPP molecules, respectively (Figure 1D). The calculated EF value of Au-SiNCA was 8.86×10^8. In order to evaluate the reproducibility based on Au-SiNCA, 4 batches of Au-SiNCA prepared at different times were used, and the Raman spectra of 10 points were randomly selected to obtain the average spectrum and the characteristic peak intensity at 998 cm^{-1} (Figure 1G). Raman spectra showed only minor differences in the intensity of characteristic peaks, demonstrating good reproducibility. Afterward, to evaluate the stability of Au-SiNCA, it was stored at room temperature for different days (1, 5, 10, and 15 days), and the intensity corresponding to the characteristic peak at 998 cm^{-1} was only reduced by 12%, showing that it was very stable (Figure 1H).

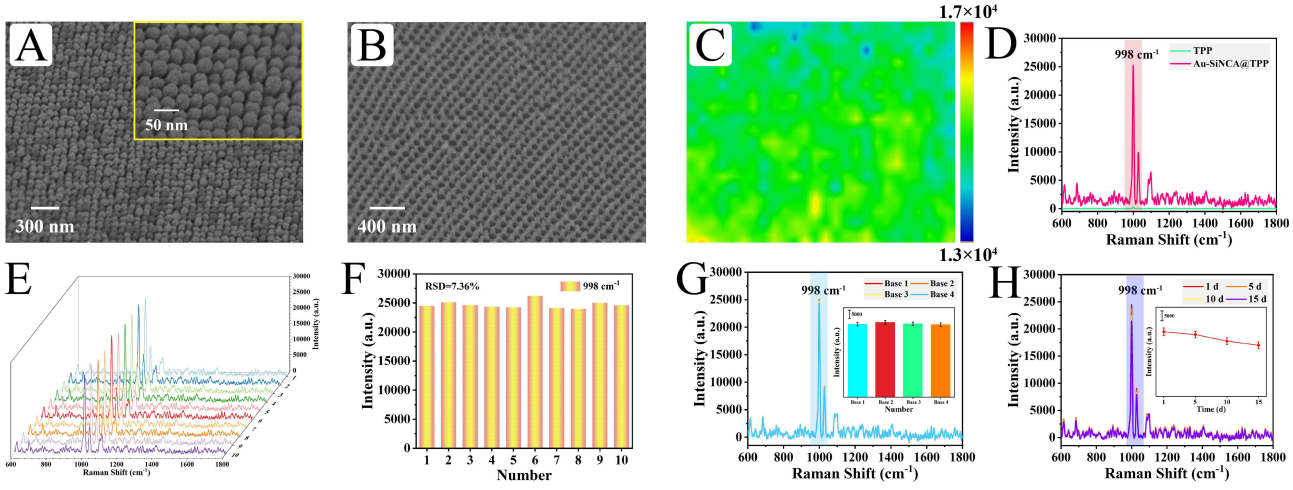

Figure 1 (**A**) SEM image and partial magnification of the incompletely etched Au-SiNCA. (**B**) SEM image of the Au-SiNCA. (**C**) SERS mapping of the Au-SiNCA modified with TPP (1×10^{-8} M). (**D**) SERS spectra of the Au-SiNCA modified with TPP (1×10^{-8} M) and of pure TPP (1×10^{-1} M). (**E**) SERS spectra of 10 randomly selected points on the surface of the TPP-labelled Au-SiNCA and (**F**) the corresponding scatter diagram of the intensity at 998 cm^{-1}. (**G**) SERS spectra of the TPP-labelled Au-SiNCA prepared in different batches and the corresponding histogram. (**H**) SERS spectra and corresponding line graphs of TPP-labelled Au-SiNCA prepared in the same batch after storage for different times.

Characterization of Au-AgNRs

The SEM image (Figure 2A) and TEM image (Figure 2B) showed that the Au-AgNRs prepared by the seed-mediated growth method were homogeneous in shape and had a rod-like structure with an aspect ratio of 3:1. HRTEM image (Figure 2C) were used to investigate further the structural characteristics of the Au-AgNRs, where the lattice spacing in Au {111} was 0.272 nm; in addition, the inset showed the SAED ring diagrams of Au-AgNRs corresponding to {111}, {200}, {220} and {311}, respectively, to surface their polycrystalline qualities. To analyze the elemental composition of Au-AgNRs, the EDX elemental mapping (Figure 2D) showed the spatial distribution of Au and Ag at different angles. Meanwhile, UV-Vis-NIR spectra showed a visible absorption band at 787 nm (Figure 2E). The EF of Au-AgNRs modified with TPP (10^{-7} M) could be calculated as 5.29×10^{6}, which showed excellent SERS performance and contributed to the SERS detection of telomerase (Figure 2F).

Experimental Feasibility Study

This experiment compared the SERS signal generated by active and inactivated telomerase to verify the feasibility of the scheme. Active telomerase, or normal telomerase, synthesizes DNA at the ends of chromosomes and is involved in cell replication. In this reaction, active telomerase triggers the SDA reaction to generate S_2 and participates in the subsequent CHA reaction to detect telomerase activity. Inactivated telomerase, on the other hand, has lost its activity due to high-temperature treatment and cannot perform its normal function. It naturally cannot trigger the SDA reaction and the subsequent CHA reaction. The same DNA concentration and reaction system were used in both systems (a and b), where inactivated telomerase was added in system b (90°C, 10 min). After the reaction, the corresponding Raman spectra are shown in Figure 3. The active telomerase produces a much higher SERS signal than the inactivated telomerase, indicating that the telomerase precursor in the system can be continuously extended to trigger subsequent reactions. On the contrary, since the inactivated telomerase cannot function, no reaction will occur in system b. In this way, the purpose of detecting telomerase activity can be achieved, which proves that the scheme is feasible.

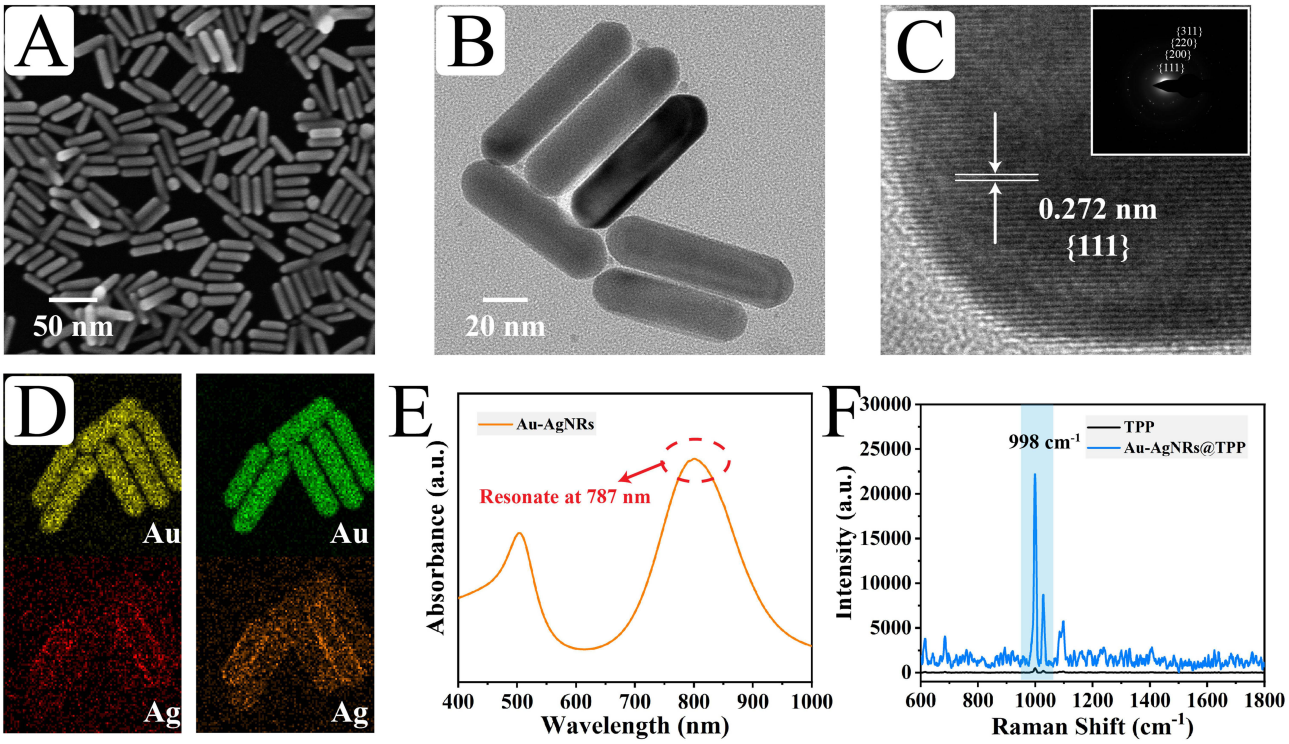

Figure 2 (**A**) SEM image and (**B**) TEM image of the Au-AgNRs. (**C**) HRTEM image and SAED pattern of the Au-AgNRs. (**D**) The EDX elemental mapping of Au element and Ag element of the Au-AgNRs. (**E**) UV-Vis-NIR spectra of the Au-AgNRs. (**F**) SERS spectra of pure TPP (1×10^{-2} M) and TPP-labelled Au-AgNRs (1×10^{-7} M).

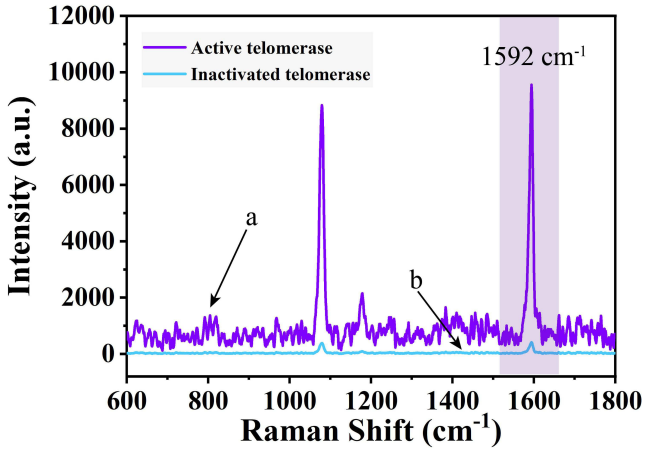

Figure 3 Raman intensity of control tests in the presence of (a) active telomerase and (b) inactivated telomerase.

Experimental Parameters Optimization

To obtain the best biosensor detection performance, the reaction conditions in the telomere extension cyclic amplification reaction system need to be optimized. As Figure 4A, as the concentration of telomerase precursor increases, the chance of collision between molecules increases, and the Raman signal is enhanced. When the telomerase precursor concentration was varied from 75 to 90 nM, the intensity of the Raman signal was almost constant. In addition, the telomerase reaction time affects the results, and the effect of telomerase decreases with time. Other conditions were kept constant, and SDA reactions were performed using telomerase precursors at a concentration of 75 nM for various times (20, 40, 60, 80, 85, 90, and 100 min). As Figure 4B, the intensity of the Raman signal varies with the reaction time and stabilizes at 85 min. Meanwhile, the enzyme reaction proceeds slowly at low temperatures. It accelerates with the increase in temperature, and the enzyme reaction is fastest when the temperature reaches the optimum temperature and then decreases with the increase in temperature. Hence, the temperature of the reaction system affects enzyme activity. As Figure 4C, the intensity of the Raman signal varies with the reaction temperature and reaches the

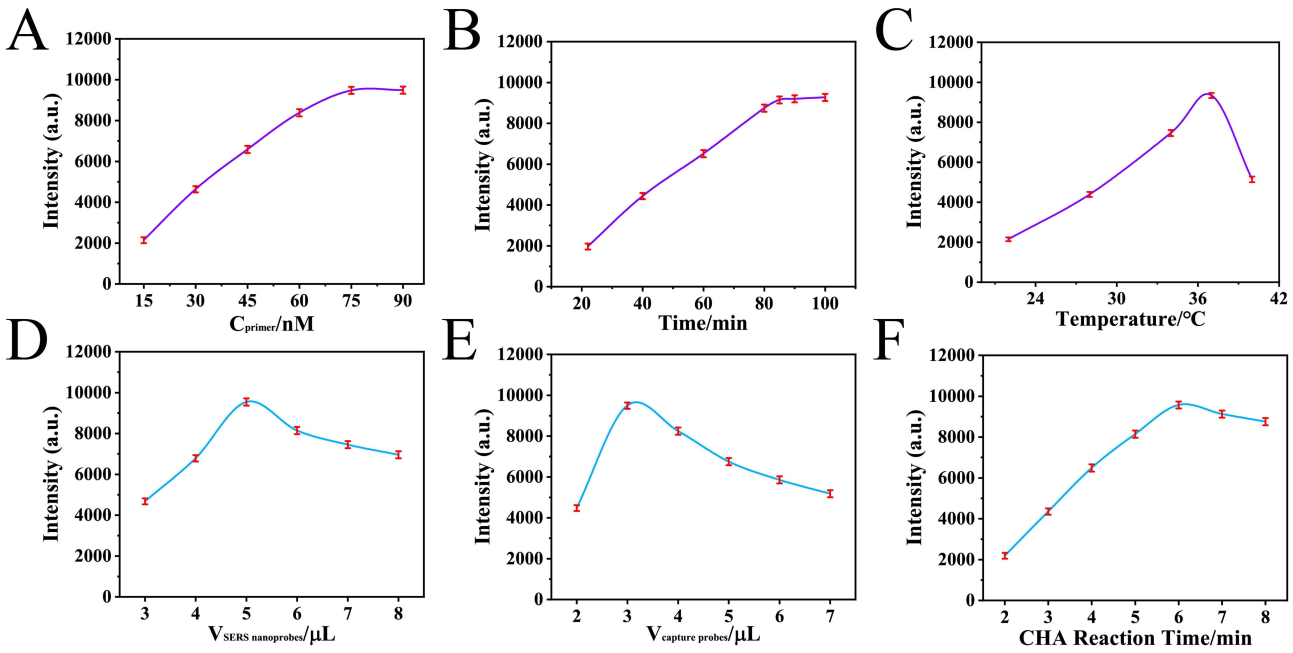

Figure 4 (**A**) Telomerase precursor concentration, (**B**) Reaction time and (**C**) Temperature of the system. (**D**) Volume of SERS nanoprobes, (**E**) Volume of SERS capture probes and (**F**) Reaction time of CHA.

maximum at 36 °C. Therefore, 75 nM was selected as the optimal concentration of telomerase precursor. The reaction time and temperature were 85 min and 36 °C, respectively, as the subsequent SDA reaction process conditions. The conditions during the CHA reaction must be optimized to amplify the SERS signal further. Since Au-SiNCA has a limited number of SERS nanoprobes and SERS capture probes that can be carried on it, their volumes need to be optimized. As shown in Figure 4D, the intensity of the Raman signal varies with the volume of SERS nanoprobes and reaches a maximum of 5 μL, indicating that Au-SiNCA can capture the SERS nanoprobes reach a maximum. Meanwhile, the SERS capture probes modified on the functionalized Au-SiNCA also affect the detection efficiency due to the volume limitation when preparing the functionalized Au-SiNCA. As in Figure 4E, the corresponding Raman signal intensity peaked at a SERS capture probe volume of 3 μL. The CHA reaction proceeded slowly with increasing time, during which the H_1-H_2 complex was gradually formed and reached the optimal detection efficiency after 6 min (Figure 4F). Therefore, 5 μL of SERS nanoprobe, 3 μL of SERS capture probe and 6 min of CHA reaction time were selected as the conditions for the subsequent CHA reaction process.

Performance Assessment

To evaluate the performance of this sensor, it was used to detect different enzymes (telomerase, lysozyme, tyrosinase, and tryptophanase) after successful preparation to investigate the specificity of its detection. As shown in Figure 5A, the Raman spectra obtained in the detection of telomerase showed an intense signal compared to other target enzymes; the difference was also highlighted by the intensity of the characteristic peak (Figure 5B) corresponding to 1592 cm^{-1} (aromatic ring respiration mode),[38] demonstrating that the sensor can effectively distinguish telomerase from complex substances, showing excellent specificity. In addition, the reproducibility of the sensor was indispensable for its practical application; therefore, the Raman spectra obtained using six different batches of the sensor for the same sample are shown in Figure 5C, and the overall waveform was consistent except for minor differences in intensity. The intensity of the characteristic peak intensity corresponding to 1592 cm^{-1} (Figure 5D) further indicates its consistency; thus, the sensor was reproducible and can be prepared in batches. For low concentrations, the detection limit of the sensor was essential, and telomerase was detected at different concentrations (1×10^{-7} IU/mL to 1×10^{-1} IU/mL) in cell lysates under optimized conditions. As shown in Figure 5E, the SERS signal intensity gradually increased with telomerase concentration. It showed a linear relationship with the concentration (Figure 5F), and the corresponding linear regression equation was y=1595.36x+11752.68 with R^2=0.9776. Therefore, the LOD of this sensor can be calculated as 8.14×10^{-6} IU/mL, which has better detection performance than other methods.

In addition, the recovery rate of telomerase in the actual test will also affect the feasibility of the protocol. Therefore, different concentrations of telomerase samples (1×10^{-3}, 1×10^{-2}, and 1×10^{-1} IU/mL) were used to carry out the test, repeated 3 times. As shown in Table 1, the recoveries of the SERS biosensor for telomerase were calculated as 97.69%, 101.35%, 98.43%, 103.22%, 97.44%, 98.16%, 97.51%, 105.73%, and 97.46%, respectively. The average recoveries were 99.67%, showing that the sensor has an excellent recovery rate of telomerase and has great feasibility for detecting telomerase activity in peripheral blood.

EMT Process Confirmed by Biological Assay

To understand the functional changes during EMT, TU686 cells were incubated with BLM for 1 h, 12 h, and 24 h. Upon analysis, the epithelial cell marker N-cadherin was gradually upregulated after BLM treatment (Figure 6A). Similarly, the fibroblast marker vimentin was upregulated by BLM treatment (Figure 6B). In addition, epithelial cell markers E-cadherin, N-cadherin, and fibroblast marker vimentin were analyzed by Western Blot to validate the EMT process (Figure 6C), and the results were consistent with those of immunofluorescence. Overall, the biological experiments provided valid support for the analysis of the EMT process using SERS spectroscopy.

Real Sample Analysis

Lysates were obtained from LC TU686 cells treated with BLM for different times (1h, 12h, and 24h), and the reliability of the device was verified by using this SERS biosensor to detect telomerase activity during EMT of LC. As the average SERS spectrum (Figure 7A) showed, the intensity of the characteristic peak corresponding to 1592 cm^{-1} gradually

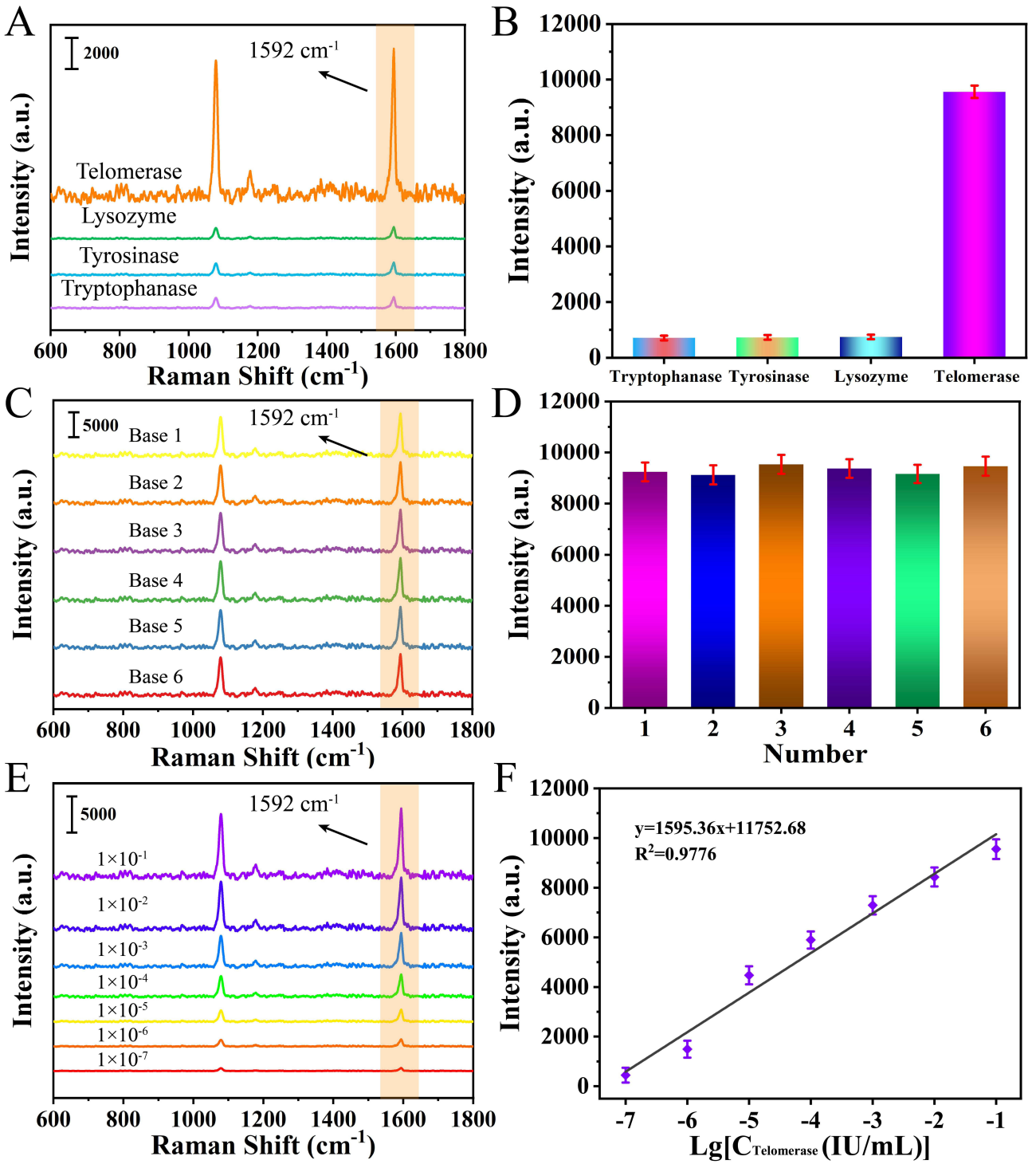

Figure 5 (**A**) SERS spectra of specific analysis for different targets: Telomerase, lysozyme, tyrosinase and tryptophanase. (**B**)The corresponding histogram of peak intensities at 1592 cm^{-1}. (**C**) SERS spectra for reproducibility analysis of different batches of SERS sensors. (**D**) The corresponding histogram of peak intensities at 1592 cm^{-1}. (**E**) SERS spectra of telomerase with different concentrations in PBS buffer (1×10^{-7}, 1×10^{-6}, 1×10^{-5}, 1×10^{-4}, 1×10^{-3}, 1×10^{-2}, and 1×10^{-1} IU/mL). (**F**) The corresponding calibration curves of SERS intensity at 1592 cm^{-1}.

increased with increasing induction time, indicating the elevation of telomerase activity during the EMT process. In addition, the corresponding histogram of the intensity of the characteristic peak showed the change in telomerase activity more clearly (Figure 7B). The telomerase activity was calculated by the correlation linear equation and compared with

Table 1 Recovery of the Biosensor Based on the Proposed Strategy

Sample Group	Added ($\times 10^{-3}$ IU/mL)	Found ($\times 10^{-3}$ IU/mL)	Recovery (%)	RSD (%)
Group 1	1	0.976	97.69	5.84
	10	10.135	101.35	5.79
	100	98.434	98.43	7.24
Group 2	1	1.032	103.22	6.85
	10	9.744	97.44	5.53
	100	98.164	98.16	6.71
Group 3	1	0.975	97.51	6.12
	10	10.573	105.73	7.53
	100	97.463	97.46	5.91

the correlation between the ELISA scheme (Table S2), and the results showed that there was no significant difference between the two protocols. Therefore, this SERS biosensor was reliable in detecting telomerase activity during EMT in LC and can be used as a potential tool for future clinical testing.

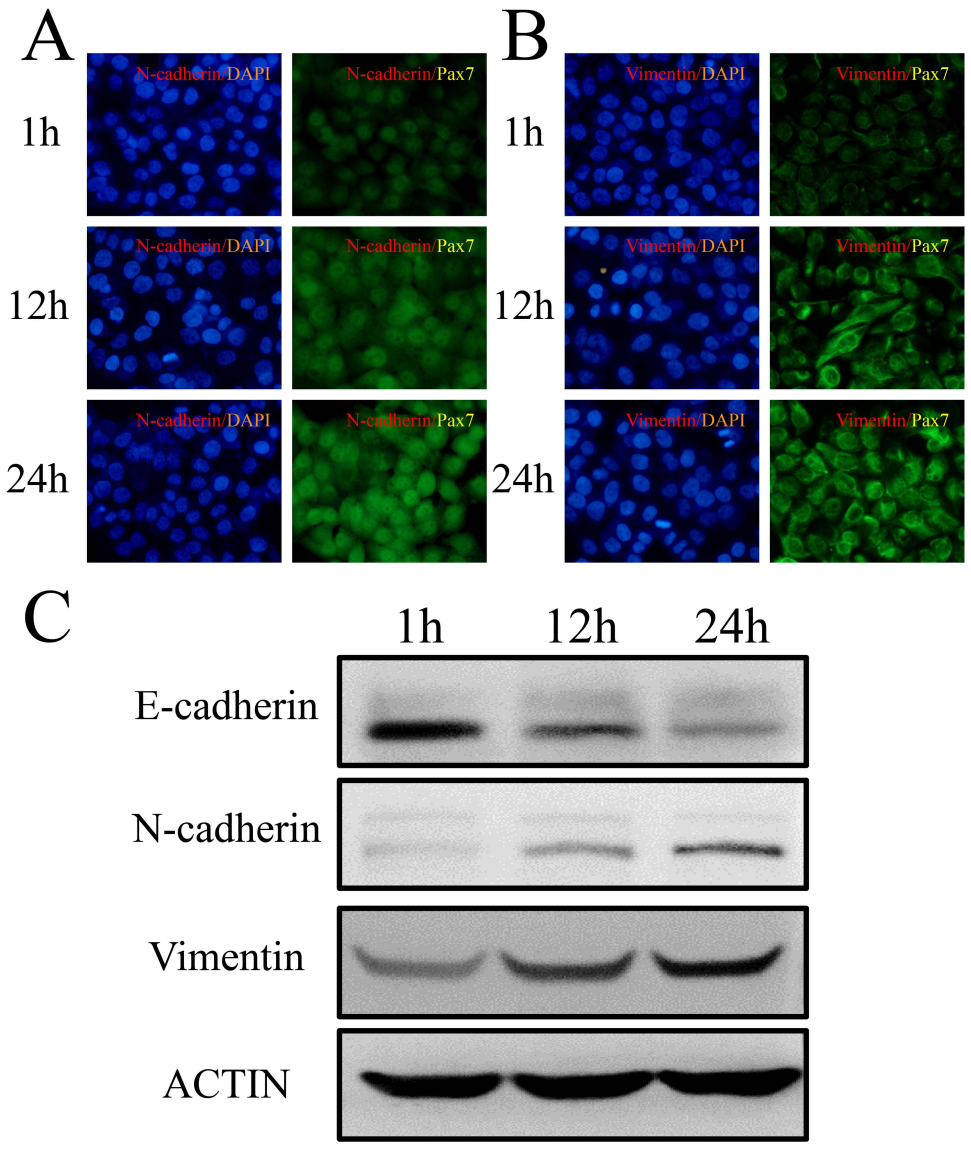

Figure 6 The expression of epithelial and fibroblast markers in TU686 cells (25 mM BLM incubation). Immunofluorescence staining was used to analyze the expression of (**A**) N-cadherin and (**B**) vimentin in TU686 cells after 1h, 12h and 24h of differentiation. (**C**) Expression of E-cadherin, N-cadherin, vimentin and ACTIN after 1h, 12h and 24h of TU686 cell differentiation was detected by immunoblotting. ACTIN was used as an internal control.

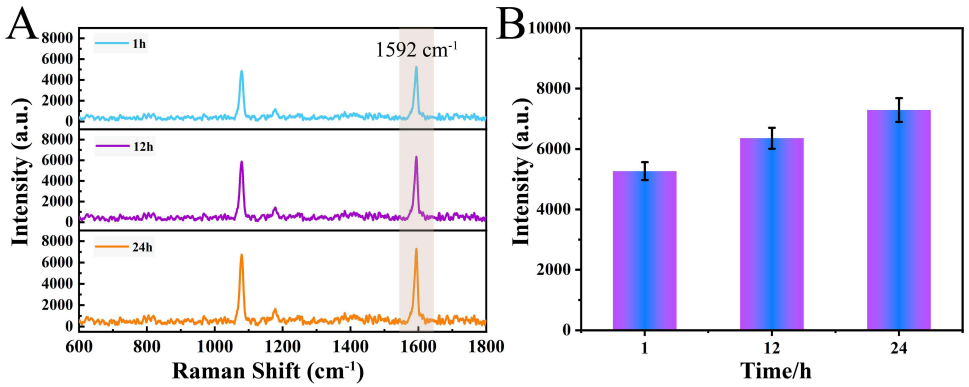

Figure 7 (**A**) Average SERS spectra of telomerase activity in TU686 cells after different times (1h, 12h, and 24h) of treatment with BLM. (**B**) The corresponding histogram of SERS signal intensity of the characteristic peak at 1592 cm^{-1}.

Conclusion

In summary, we prepared a novel SERS biosensor based on functionalized Au-SiNCA, using the SDA-CHA strategy as a signal amplification method for the ultrasensitive detection of telomerase during EMT of LC. The labeled probes (Au-AgNRs) and the capture substrate (Au-SiNCA) exhibit good Raman signal enhancement performance in this scheme. Based on this, the SERS biosensor has a shallow detection limit (8.14×10^{-6} IU/mL) while having excellent specificity and reproducibility, which has obvious advantages over previously reported detection methods. In addition, biological experiments' surface using BLM to treat LC TU686 cells helps to study the functional changes of different processes of EMT. The results of the ELISA scheme also confirmed the sensitivity of the scheme for telomerase activity during EMT of LC. Therefore, this SERS biosensor provides a reproducible, selective and ultrasensitive method for telomerase detection, showing great potential for early screening of LC in clinical applications.

Acknowledgments

This study was financially supported by grants from the National Natural Science Foundation of China (Project code: 81403232); the Major Programs of Natural Science Foundation of higher education in Jiangsu Province (19KJA480003), the Natural Science Foundation of Jiangsu Province (No. BK20171290), the Maternal and Child Health Research Project of Jiangsu Province (F202124), the Administration of Traditional Chinese Medicine Project of Jiangsu Province (MS2021081), the Natural Science Foundation of Yangzhou (YZ2021087).

Disclosure

There are no conflicts to declare.

References

1. Azam MA, Sampieri C, Ioppi A, et al. Deep learning applied to white light and narrow band imaging videolaryngoscopy: toward real-time laryngeal cancer detection. *Laryngoscope*. 2022;132(9):1798–1806. doi:10.1002/lary.29960
2. Sahoo PK, Mishra S, Panigrahi R, Bhoi AK, Barsocchi P. An improvised deep-learning-based mask R-CNN model for laryngeal cancer detection using CT images. *Sensors*. 2022;22(22):8834. doi:10.3390/s22228834
3. Ohkubo J-I, Wakasugi T, Takeuchi S, Takahashi A, Nguyen TN, Suzuki H. Biophysical properties of the neck skin indicating potential complications of salvage surgery for laryngeal/hypopharyngeal cancer. *Acta Otolaryngol*. 2022;142(7–8):634–637. doi:10.1080/00016489.2022.2117411
4. Zhao N, Liu H, Zhang A, Wang M. Expression levels and clinical significance of miR-203 and miR-133b in laryngeal carcinoma. *Oncol Lett*. 2020;20(5):1. doi:10.3892/ol.2020.12076
5. Georgakopoulos-Soares I, Chartoumpekis DV, Kyriazopoulou V, Zaravinos A. EMT factors and metabolic pathways in cancer. *Front Oncol*. 2020;10 (499). doi:10.3389/fonc.2020.00499
6. Huang R, Zong X. Aberrant cancer metabolism in epithelial-mesenchymal transition and cancer metastasis: mechanisms in cancer progression. *Crit Rev Oncol Hemat*. 2017;115:13–22. doi:10.1016/j.critrevonc.2017.04.005
7. Cornean CI, Maniu AA. Analysis of TERT Rs2736100 genotype distribution in laryngeal squamous cell carcinoma patients. *J Med Life*. 2022;15 (9):1191–1197. doi:10.25122/jml-2022-0114
8. Wei X, Liu F, Jiang X, Xu X, Zhou T, Kang C. YY1 promotes telomerase activity and laryngeal squamous cell carcinoma progression through impairment of GAS5-mediated p53 stability. *Front Oncol*. 2021;11:145.

9. Brousset P, Al Saati T, Chaouche N, Zenou RC, Mazerolles C, Delsol G. Techniques for detection of telomerase activity in tissue samples. Diagnostic and prognosis importance. *Ann Pathol*. 1997;17(5):364–368.
10. Liu D, La M. Electrochemical, electrochemiluminescent and photoelectrochemical methods for detection of telomerase activity: a review. *Int J Electrochem Sci*. 2020;15(11):11371–11386. doi:10.20964/2020.11.28
11. Wang R, Li J, Jin R, Ye Q, Cheng L, Liu R. Nonradioactive direct telomerase activity detection using biotin-labeled primers. *J Clin Lab Anal*. 2021;35(6):123.
12. Chen X, Deng Y, Cao G, et al. An ultrasensitive and point-of-care sensor for the telomerase activity detection. *Anal Chim Acta*. 2021;1146:61–69. doi:10.1016/j.aca.2020.11.037
13. Ma Y, Mao G, Wu G, Fan J, He Z, Huang W. A novel nano-beacon based on DNA functionalized QDs for intracellular telomerase activity monitoring. *Sens Actuators B Chem*. 2020;304:127385. doi:10.1016/j.snb.2019.127385
14. Li N, Hao Z, Cao H, et al. Acupressure mat-like nanostructure with improved SERS performance. *Opt Laser Technol*. 2022;148:107765. doi:10.1016/j.optlastec.2021.107765
15. Liu H, Gao X, Xu C, Liu D. SERS tags for biomedical detection and bioimaging. *Theranostics*. 2022;12(4):1870–1903. doi:10.7150/thno.66859
16. Fu Q, Liu HL, Wu Z, et al. Rough surface Au@Ag core-shell nanoparticles to fabricating high sensitivity SERS immunochromatographic sensors. *J Nanobiotechnology*. 2015;13. doi:10.1186/s12951-015-0142-0
17. Sun Y, Fang L, Yi Y, Feng A, Zhang K, Xu -J-J. Multistage nucleic acid amplification induced nano-aggregation for 3D hotspots-improved SERS detection of circulating miRNAs. *J Nanobiotechnology*. 2022;20(1). doi:10.1186/s12951-022-01500-y
18. Chen R, Sun Y, Huo B, et al. Development of Fe3O4@Au nanoparticles coupled to Au@Ag core-shell nanoparticles for the sensitive detection of zearalenone. *Anal Chim Acta*. 2021;1180:338888. doi:10.1016/j.aca.2021.338888
19. Ryu H-J, Lee WK, Kim YH, Lee J-S. Interfacial interactions of SERS-active noble metal nanostructures with functional ligands for diagnostic analysis of protein cancer markers. *Microchim Acta*. 2021;188(5). doi:10.1007/s00604-021-04807-z
20. Wen C, Wang L, Liu L, Shen X-C, Chen H. Surface-enhanced raman probes based on gold nanomaterials for in vivo diagnosis and imaging. *Chem Asian J*. 2022;17(7). doi:10.1002/asia.202200014
21. Bian X, Zhang G, Liu B, Yang J. One-pot synthesis of Au/Ag alloy@SiO2 core-shell nanoparticles and their metal-enhanced fluorescence and surface-enhanced Raman scattering spectroscopies. *J Nanopart Res*. 2022;24(2). doi:10.1007/s11051-022-05412-8
22. Huang HJ, Shiao M-H, Lin Y-W, et al. Au@Ag dendritic nanoforests for surface-enhanced raman scattering sensing. *Nanomaterials*. 2021;11(7):45.
23. Wei W, Yu D, Du Y, Ding Y, Huang Q. One-step fabrication of Au-Ag alloys and its application for catalysts and SERS sensors. *Spectrochim Acta A Mol Biomol Spectrosc*. 2022;267:120476. doi:10.1016/j.saa.2021.120476
24. Chen S-Y, Yang M, Liu X-Y, Zha L-S. Study on Au@Ag core-shell composite bimetallic nanorods loading filter paper as SERS substrate. *Spectrosc Spect Anal*. 2018;38(6):1747–1752.
25. Wei J, Kan C, Lou Y, Ni Y, Xu H, Wang C. Synthesis and stability of bimetallic Au@Ag nanorods. *Superlattices Microstruct*. 2016;100:315–323. doi:10.1016/j.spmi.2016.09.046
26. Zhang PP, Gao J, Sun XH. An ultrasensitive, uniform and large-area surface-enhanced Raman scattering substrate based on Ag or Ag/Au nanoparticles decorated Si nanocone arrays. *Appl Phys Lett*. 2015;106(4):1245.
27. Cao Y, Ma C, Zhu -J-J. DNA technology-assisted signal amplification strategies in electrochemiluminescence bioanalysis. *J Anal Test*. 2021;5 (2):95–111. doi:10.1007/s41664-021-00175-y
28. Li T, Duan R, Duan Z, Huang F, Xia F. Fluorescence signal amplification strategies based on DNA nanotechnology for miRNA detection. *Chem Res Chin Univs*. 2020;36(2):194–202. doi:10.1007/s40242-019-0031-4
29. Zhou C, Zou H, Sun C, Ren D, Chen J, Li Y. Signal amplification strategies for DNA-based surface plasmon resonance biosensors. *Biosens Bioelectron*. 2018;117:678–689. doi:10.1016/j.bios.2018.06.062
30. Simmel FC, Yurke B, Singh HR. Principles and applications of nucleic acid strand displacement reactions. *Chem Rev*. 2019;119(10):6326–6369. doi:10.1021/acs.chemrev.8b00580
31. Zhou H, Zhang J, Li B, Liu J, Xu -J-J, Chen H-Y. Dual-mode SERS and electrochemical detection of miRNA based on popcorn-like gold nanofilms and toehold-mediated strand displacement amplification reaction. *Anal Chem*. 2021;93(15):6120–6127. doi:10.1021/acs.analchem.0c05221
32. Wang H, Wang H, Wu Q, Liang M, Liu X, Wang F. A DNAzyme-amplified DNA circuit for highly accurate microRNA detection and intracellular imaging. *Chem Sci*. 2019;10(41):9597–9604. doi:10.1039/C9SC03552D
33. Yang M, Li H, Li X, Huang K, Xu W, Zhu L. Catalytic hairpin self-assembly regulated chameleon silver nanoclusters for the ratiometric detection of CircRNA. *Biosens Bioelectron*. 2022;209:114258. doi:10.1016/j.bios.2022.114258
34. Wu Y, Li Y, Han H, Zhao C, Zhang X. Dual cycle amplification and dual signal enhancement assisted sensitive SERS assay of MicroRNA. *Anal Biochem*. 2019;564:16–20. doi:10.1016/j.ab.2018.10.004
35. Xiao F, Liu J, Guo Q, et al. Dual-signal amplification strategy for sensitive MicroRNA detection based on rolling circle amplification and enzymatic repairing amplification. *ACS Omega*. 2020;5(50):32738–32743. doi:10.1021/acsomega.0c05141
36. Zhao W, Liu X, Luo L, Li L, You T. A sensitive electrochemiluminescence aptasensor for Pb2+ detection in soil based on dual signal amplification strategy of aggregation-induced emission and resonance energy transfer. *Electrochim Acta*. 2022;421:140463. doi:10.1016/j.electacta.2022.140463
37. Sandhyarani N, Pradeep T. Ion/surface reactions at monolayers in solution: a combined surface enhanced Raman-X-ray photoelectron spectroscopic investigation of the chemical modification of a 2-mercaptobenzothiazole monolayer on polycrystalline Au films. *J Colloid Interf Sci*. 1999;218 (1):176–183. doi:10.1006/jcis.1999.6402
38. Yang L, Xu L, Wu X, et al. Atomic force microscope guided SERS spectra observation for Au@Ag-4MBA@PVP plasmonic nanoparticles. *Molecules*. 2019;24(20):3789. doi:10.3390/molecules24203789